Environmental Pollution 363 (2024) 125227

Contents lists available at ScienceDirect

Environmental Pollution

journal homepage: www.elsevier.com/locate/envpol

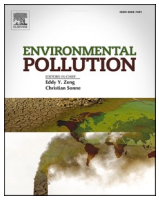

Spatiotemporal variations of $PM_{2.5}$ organic molecular markers in five central cities of the Yangtze River Delta, East China in autumn and winter: Implications for regional and local sources of organic aerosols☆

Wei Feng [a], Guihong Dong [a], Wanqing Qi [a], Yizhen Wang [a], Xiangyu Zhang [a], Ke Li [a], Hong Liao [a], Yuhang Wang [b], Zhijuan Shao [c], Mingjie Xie [a,*]

[a] Collaborative Innovation Center of Atmospheric Environment and Equipment Technology, Jiangsu Key Laboratory of Atmospheric Environment Monitoring and Pollution Control, School of Environmental Science and Engineering, Nanjing University of Information Science & Technology, 219 Ningliu Road, Nanjing, 210044, China

[b] School of Earth and Atmospheric Sciences, Georgia Institute of Technology, Atlanta, GA, 30332, United States

[c] School of Environment Science and Engineering, Suzhou University of Science and Technology Shihu Campus, 99 Xuefu Road, Suzhou, 215009, China

ARTICLE INFO

Keywords:
Organic aerosol
Organic molecular marker
Spatial distribution
Regional influence
Source apportionment

ABSTRACT

Information on the spatiotemporal variations in the composition and sources of organic aerosols (OA) is needed to identify regional influences and to establish effective control measures. Here, 23-h $PM_{2.5}$ samples were collected in five central cities of the Yangtze River Delta in eastern China, including Nanjing, Suzhou, Wuxi, Changzhou, and Zhenjiang, every three days from 2020/09/01 to 2021/02/28. Each sample was analyzed for water-soluble inorganic ions, organic carbon (OC), elemental carbon (EC), and organic molecular markers (OMMs). Generally, the major components of $PM_{2.5}$, including NH_4^+, SO_4^{2-}, NO_3^-, OC, and EC, exhibited similar temporal patterns across the five cities. In all OMM groups, the concentrations of PAHs, oxygenated PAHs, and secondary products of isoprene showed strong correlations ($r = 0.79 \pm 0.050$–0.93 ± 0.028) and low coefficient of divergence (COD $= 0.22 \pm 0.024$–0.30 ± 0.033) between sampling sites, indicating a homogeneous spatial distribution of industrial emissions and biogenic secondary OA in autumn and winter. Other OMMs showed wider r (e.g., steranes and hopanes, 0.20–0.80) and COD (0.26–0.69) ranges for all site pairs, probably due to the influence of local emissions. Based on the source apportionment results using Positive matrix factorization, the biomass burning factor dominated the contribution to OC and EC in winter and showed strong correlations ($r = 0.84 \pm 0.063$) between the sampling sites, indicating regional transport of emissions from biomass burning and fossil fuel combustion in the heating season. Traffic-related factors had the greatest spatial heterogeneity ($r = 0.27 \pm 0.19$–0.51 ± 0.16) and contributed significantly to OC at their maximum levels.

1. Introduction

Organic aerosols (OA) consist of a complex mixture of compounds and make up 20–90% of particulate matter of less than 2.5 μm diameter ($PM_{2.5}$; Zhang et al., 2007; Hallquist et al., 2009; Jimenez et al., 2009). The effects of OA on health and climate have been extensively investigated in recent decades (Maria et al., 2004; Mauderly and Chow, 2008; Pye et al., 2021; Jo et al., 2023). Deciphering the physicochemical features and atmospheric processes of OA depends to a large extent on how well they are characterized (Nozière et al., 2015). Several groups of semi-volatile organic compounds (SVOCs; e.g., *n*-alkanes, PAHs, and anhydro sugars) were well known as organic molecular markers (OMMs) in receptor-based source apportionment studies (Jaeckels et al., 2007; Lewandowski et al., 2008; Shrivastava et al., 2007). The recognized sources of secondary OA (SOA) were attributed to the transformation of volatile organic compounds (VOCs) during regional transport, and contributions from primary sources were expected to be associated with local emissions (e.g., motor vehicle emissions). Based on the source apportionment results, regulatory strategies were developed to control regional or local pollution. For example, leak detection in the petrochemical industry and the use of low-VOC adhesives and paints have been promoted to reduce SOA and ozone formation (Wei et al., 2011;

☆ This paper has been recommended for acceptance by Eddy Y. Zeng.

* Corresponding author., Mailing address: 219 Ningliu Road, Nanjing, Jiangsu, 210044, China.
E-mail addresses: mingjie.xie@nuist.edu.cn, mingjie.xie@colorado.edu (M. Xie).

https://doi.org/10.1016/j.envpol.2024.125227
Received 13 August 2024; Received in revised form 27 September 2024; Accepted 30 October 2024
Available online 31 October 2024

Zhang et al., 2022), as well as smart traffic management systems and low-dust construction to control emissions from local traffic-related and dust sources (Wu et al., 2016; Padrón et al., 2022). However, emissions from multiple primary sources, such as biomass burning, fossil fuel combustion, and dust, can mix and undergo long-range transport (Zhou et al., 2018; Mukherjee et al., 2022), which then increases local $PM_{2.5}$ pollution for the specific study location. Therefore, the results of source apportionment determined at single sites cannot distinguish between regional and local sources.

Given the spatial variability of $PM_{2.5}$ constituents and their sources, the representativeness of $PM_{2.5}$ characterization and source apportionment at a single site has always been questioned. In previous studies, multiple-site sampling and measurements of $PM_{2.5}$ were conducted mostly at the city level (Krudysz et al., 2009; Xie et al., 2012a; Chow et al., 2022). Kim et al. (2005) showed that the spatial distribution of $PM_{2.5}$ elements and the contributions of local source categories (e.g., incinerators and cement kilns) were highly heterogeneous in St. Louis, United States, which could lead to exposure misclassification in epidemiologic studies where health outcomes were regressed over the time series of $PM_{2.5}$ components and source contributions. However, the spatial distribution of OA and its sources based on measurement results at the regional level has rarely been assessed (Zheng et al., 2006; Golly et al., 2019; Zheng et al., 2024). According to the available studies, biomass burning and the formation of SOA are major OA sources at the regional scale, although significant differences in source contribution distributions between urban and rural sites have been found.

The southern part of Jiangsu province in eastern China consists of Nanjing, Suzhou, Wuxi, Changzhou, and Zhenjiang, which are the central cities of the Yangtze River Delta. According to the Jiangsu Provincial Bureau of Statistics of China (2023), these five cities have an area of 28084 km^2 and a permanent population of 38.5 million in 2022, accounting for 26.3% and 45.2% of the total area and population of Jiangsu province, respectively. The total gross domestic product (GDP) of southern Jiangsu amounted to 70.28 trillion yuan in 2022, comparable to that of Zhejiang province (77.7 trillion yuan) and more than 50% higher than that of Shanghai (44.7 trillion yuan) — two neighboring developed areas in the Yangtze River Delta. Industry accounted for 40.8% of GDP in southern Jiangsu, and the industrial electricity consumption (2.8 trillion kWh) and highway passenger traffic (257 million) in this area dominated (60.2% and 78.8%) the entire Jiangsu province in 2022. Considering the high urbanization rate (80.2%) in southern Jiangsu, the urban areas in the above five cities can represent the highly developed region in the Yangtze River Delta.

$PM_{2.5}$ pollution in the Yangtze River Delta is a major concern and is usually associated with biomass burning, industrial and vehicle emissions, construction activities, and unfavorable weather conditions (Yang et al., 2018; Zhang et al., 2020). As reported by the Chinese Ministry of Ecology and Environment (https://www.mee.gov.cn/hjzl/dqhj/qgkqzlzk/), the annual average concentrations of $PM_{2.5}$ in the Yangtze River Delta in 2021–2023 (31–32 μm^{-3}) remained below the Class II limit (35 μm^{-3}) of China's National Ambient Air Quality Standards (NAAQS) after the implementation of the "Air Pollution Prevention and Control Action Plan" (2013–2017) and the "Three-Year Blue Sky Action Plan" (2018–2020), but the average $PM_{2.5}$ concentrations in the winter months (December, January, and February) were always above 35 μm^{-3} (38–66 μm^{-3}) after 2020. Before implementing joint prevention and control measures at the regional level involving cooperation between local governments, industries, communities, and environmental authorities, information on the spatial distribution of $PM_{2.5}$ composition is needed, especially for OA where a significant proportion comes from primary emissions, to determine regional sources and their contributions. However, there are very few measurement studies on the spatial distribution of OA composition and sources in the Yangtze River Delta. Since $PM_{2.5}$ pollution in eastern China occurs more frequently in autumn and winter than in spring and summer (Zhang and Cao, 2015; Sun et al., 2019; Guo et al., 2020a), this work collected filter samples of ambient $PM_{2.5}$ in five central cities of the Yangtze River Delta from September 1, 2020 to February 28, 2021. Water-soluble inorganic ions (WSIIs), organic carbon (OC), elemental carbon (EC), and a matrix of OMMs were speciated and compared among the cities to assess their spatial distribution. Finally, the OMM data were pre-selected for a positive matrix factorization (PMF) analysis, and regional and local OA sources were distinguished by analyzing the spatial variability of the time series of source contributions. The study results will benefit regional cooperation in the continuous reduction of $PM_{2.5}$ pollution in the Yangtze River Delta.

2. Methods

2.1. $PM_{2.5}$ sampling

From January 09, 2020 to 02/28/2021, 23-h $PM_{2.5}$ samples (10:00–9:00 a.m. the next day) were collected simultaneously every third day in Nanjing, Suzhou, Wuxi, Changzhou, and Zhenjiang, and the sampling frequency is about twice that of many previous studies on spatiotemporal variations of OMMs and OA (Krudysz et al., 2009; Cheung et al., 2012; Xie et al., 2012a, b; Chow et al., 2022; Zheng et al., 2024). The locations and sample numbers of the five sampling sites are shown in Fig. 1. All five sites are located in urban areas, and the surrounding pollutant sources are mainly residential areas and traffic emissions. A four-channel sampler (TH-16a, Wuhan Tianhong, China) was set up at each site to collect $PM_{2.5}$ samples at a flow rate of 16.7 L min^{-1}. Two Teflon and two quartz filters (47 mm diameter) were installed for $PM_{2.5}$ sampling. Samples on the Teflon filters were analyzed for WSIIs; OC, EC, and OMMs were determined from the quartz filter samples. Field blanks were taken each month to correct for possible contamination. All samples were stored in the dark at −20 °C before chemical analysis. During the whole sampling period, the temperature (°C) and relative humidity (RH, %) were recorded for each sampling day (Fig. S1), and the concentrations of the six criteria air pollutants ($PM_{2.5}$, PM_{10}, SO_2, CO, NO_2, and MDA8 O_3; Fig. S1) defined in the Chinese NAAQS were retrieved from the online platform for monitoring and analyzing air quality in China (Wang, 2013) for each city.

2.2. Chemical characterization

The analytical methods for WSIIs, OC, EC, and OMMs in $PM_{2.5}$ samples were described in previous studies (Gou et al., 2021; Yang et al., 2021; Qin et al., 2021). WSIIs were extracted from Teflon filter samples using ultrapure water (18.2 MΩ) and analyzed by ion chromatography. The recoveries of our target WSIIs (NH_4^+, NO_3^-, SO_4^{2-}, K^+, and Ca^{2+}) were in the range of 95.6 ± 1.76%–105 ± 5.86% with detection limits of less than 0.1 μg m^{-3} (0.016–0.088 μg m^{-3}). A ~0.5 cm^2 aliquot of each quartz filter was analyzed for OC and EC using a thermo-optical carbon aerosol analyzer (DRI model 2015) according to the IMPROVE-A protocol. The DRI OC-EC analyzer was calibrated daily with the standard solution of sucrose (5–15 μgC μL^{-1}), and the detection limits of OC and EC were 0.40 and 0.20 μg m^{-3}, respectively. After adding deuterated PAH solutions as internal standards (IS), two aliquots of each quartz filter were extracted with dichloromethane (DCM) and a DCM/methanol mixture (1:1, v:v), respectively. After filtration, the DCM extracts were rotary evaporated and blown down to ~200 μL for analysis of non-polar OMM using a gas chromatograph (GC, Agilent 7890B)-mass spectrometer (MS, Agilent 5977B). The DCM/methanol extracts were evaporated to dryness and reacted with N, O-bis(trimethylsilyl)trifluoroacetamide (BSTFA) at 70 °C for 3 h to convert the polar OMMs into trimethylsilyl ethers and esters for GC-MS analysis. Table S1 contains information on the non-polar and polar OMMs. All OMMs were quantified using six-point calibration curves following the internal standard method and corrected for field blank values. The recoveries of the authentic standards for non-polar (*n*-alkanes, PAHs, steranes, and hopanes) and polar species (cis-ketopinic acid, anhydrosugars, and sugar polyols; Table S1)

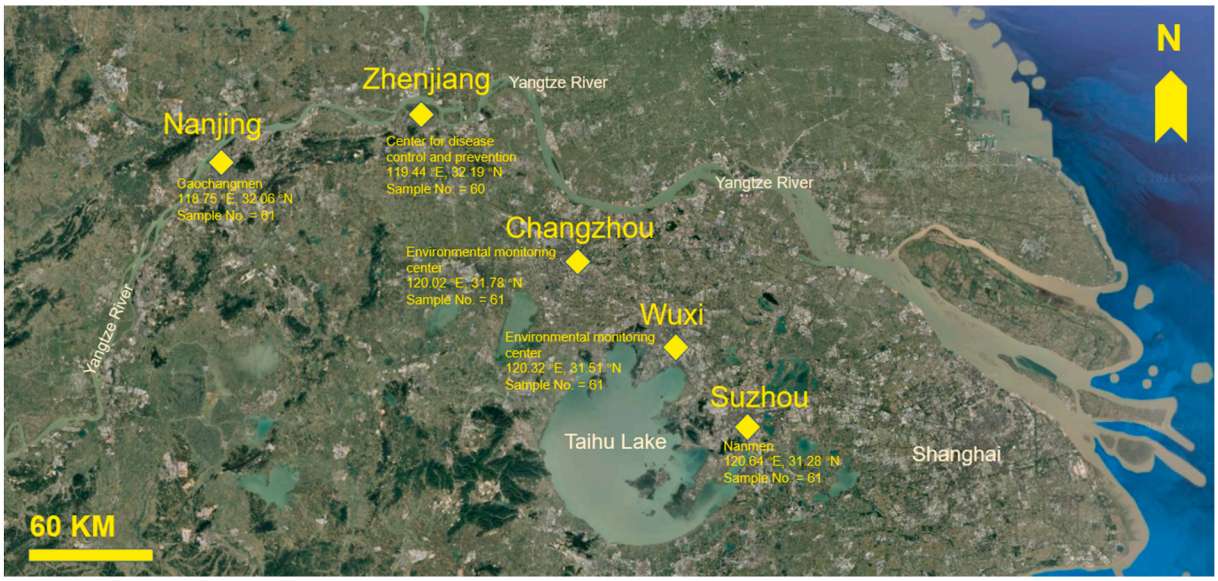

Fig. 1. Locations of sampling sites in five central cities of the Yangtze River Delta, eastern China. Map data: Google Maps.

were in the ranges of 81.8 ± 8.89%–112 ± 10.9% and 67.2 ± 3.50%–107 ± 2.65%, respectively, and the corresponding detection limits were in the ranges of 0.012–0.35 ng m^{-3} and 0.14–0.71 ng m^{-3}. The measurement results of the $PM_{2.5}$-bound OMMs were not adjusted by recoveries.

2.3. PMF analysis

The EPA PMF 5.0 model was applied to identify and quantify the sources of $PM_{2.5}$ major components, especially for OC, in the five cities. Besides NH_4^+, NO_3^-, SO_4^{2-}, OC, and EC, Ca^{2+} and K^+ data were also included as they are commonly used as source indicators for dust and biomass burning, respectively (Huang et al., 2010; Urban et al., 2012; Fourtziou et al., 2017). The OMM input data were pre-selected based on the uniqueness of the source makers, the proportion of valid measurements (>30%), and the interpretability of the output base-case solutions (Xie et al., 2013; Feng et al., 2023). Due to the limited number of $PM_{2.5}$ samples available at each site ($N = \sim 61$), all sample data from the five cities were pooled for PMF analysis. However, the samples that did not contain OMM data were omitted. This resulted in a data set with 296 observations of 48 species (7 bulk components and 41 OMMs). The final factor number was determined primarily by referring to the physical meaningfulness of the output factors. In addition, the robustness of PMF solutions with 4–10 factors and their Q/Q_{exp} values were also considered (Table S2). Further details on the preparation of the input data set and the determination of the factor number for the PMF analysis are provided in Text S1 in Supporting Information.

2.4. Assessment of spatial variability

The correlation coefficient (r) and the coefficient of divergence (COD) were calculated to assess the spatial variability of $PM_{2.5}$ component concentrations and source contributions. The correlation coefficient is used to measure how the same species or sources vary together at two sampling sites, and the COD helps determine how different locations diverge in terms of species concentrations or source contributions, and is defined by the following formula

$$COD_{fh} = \sqrt{\frac{1}{n}\sum_{i=1}^{n}\left(\frac{x_{if} - x_{ih}}{x_{if} + x_{ih}}\right)^2} \quad (1)$$

where x_{if} and x_{ih} are the concentrations of the same species or the contributions from the same source for the ith sampling day at sites f and h, and n is the number of sample pairs. A COD value of 0 indicates complete similarity between the two sampling sites, while a value close to 1 suggests complete differences.

3. Results and discussion

3.1. Overview of bulk speciation

NO_3^- was the most abundant $PM_{2.5}$ species in all five cities (9.54 ± 10.1–12.1 ± 11.3 μg m^{-3}; Table 1) during the sampling campaign, accounting for an average of 30.0 ± 12.8% to 34.5 ± 12.0% of reconstructed $PM_{2.5}$ ($rPM_{2.5}$) — the sum of all bulk components. As shown in Fig. S2, SO_4^{2-}, NO_3^-, and NH_4^+ (SNA) dominated the $PM_{2.5}$ composition, especially after the heating season in northern China started on November 15, 2020. The mean contributions of NO_3^- to $rPM_{2.5}$ in the five cities with $rPM_{2.5} > 35$ μg m^{-3} (Class II limit value for $PM_{2.5}$ in the Chinese NAAQS) during the heating season ranged from 36.3 ± 7.39% to 47.3 ± 4.61%, significantly higher ($p < 0.05$) than the mean values of the remaining observations (24.8 ± 11.2% to 29.7 ± 10.5%). Since the equivalent ratios of NH_4^+ to SO_4^{2-}+NO_3^- were always close to unity, the sharp increase in $rPM_{2.5}$ after November 15, 2020 was directly caused by the rapid formation of NH_4NO_3. The average OC concentrations were comparable to or higher than those of NH_4^+ and SO_4^{2-}, contributing an average of 18.7 ± 7.39%–26.7 ± 8.45% to $rPM_{2.5}$ (Table 1), indicating a necessity in controlling OA emissions and formation to further mitigate $PM_{2.5}$ pollution in the Yangtze River Delta in autumn and winter.

Fig. S3 compares the concentration time series of individual bulk species in the five cities, and all components show similar temporal variations. Only Ca^{2+}, OC, and EC were obviously higher at their peak values in Changzhou than in the other four cities (Figs. S3c, f, and g). Since the combustion-related carbonaceous aerosols can mix with surface dust and be resuspended (Xie et al., 2022a; Feng et al., 2023), the sampling site in Changzhou may be more affected by dust resuspension than the other four sites. The average concentrations of $rPM_{2.5}$, which is dominated by SNA, showed no significant differences ($p > 0.05$) among the sampling sites, and the time series of SNA and $rPM_{2.5}$ in the five cities almost overlapped (Figs. S3a, d, e, and h). Except for Ca^{2+}, $PM_{2.5}$ bulk species had high r (mean, 0.78 ± 0.10–0.90 ± 0.05) and low COD (0.15 ± 0.03–0.24 ± 0.04) values between sampling sites (Fig. 2), indicating high spatial homogeneity for $PM_{2.5}$ major components. Therefore, $PM_{2.5}$ pollution in the center of the Yangtze River Delta during the heating

Table 1
Statistics for the concentrations of $PM_{2.5}$ bulk components (μg m^{-3}) and OMM groups (ng m^{-3}) in five central cities of the Yangtze River Delta.

	Nanjing		Suzhou		Wuxi		Changzhou		Zhenjiang	
	Median	Mean ± stdev	Median	Mean ± stdev	Median	Mean ± stdev	Median	Mean ± stdev	Median	Mean ± stdev
Bulk components										
NH_4^+	3.79	5.22 ± 3.86	3.54	4.32 ± 3.51	3.73	4.61 ± 3.45	3.50	4.58 ± 2.99	3.90	4.92 ± 3.98
K^+	0.33	0.40 ± 0.19	0.27	0.31 ± 0.18	0.32	0.39 ± 0.21	0.39	0.42 ± 0.20	0.39	0.43 ± 0.20
Ca^{2+}	0.19	0.23 ± 0.12	0.16	0.22 ± 0.15	0.16	0.21 ± 0.11	0.33	0.40 ± 0.30	0.16	0.22 ± 0.15
NO_3^-	7.92	12.1 ± 11.3	6.21	9.54 ± 10.1	6.87	10.0 ± 10.1	7.69	10.8 ± 9.15	7.28	10.9 ± 11.4
SO_4^{2-}	4.72	5.57 ± 3.24	4.08	4.69 ± 3.33	4.53	5.01 ± 3.15	4.33	5.05 ± 3.06	4.54	5.42 ± 3.41
OC	4.27	4.81 ± 2.64	4.48	5.03 ± 2.70	4.77	5.37 ± 3.12	6.88	8.09 ± 5.17	4.94	5.48 ± 2.50
EC	1.60	1.92 ± 1.33	1.48	1.95 ± 1.53	1.75	2.26 ± 1.70	2.17	2.97 ± 2.47	2.13	2.49 ± 1.47
$rPM_{2.5}$[a]	21.9	30.1 ± 20.7	21.1	26.0 ± 19.6	22.0	27.8 ± 20.1	27.4	32.3 ± 20.5	23.3	29.8 ± 21.3
OC%[b]	17.8	18.7 ± 7.39	22.6	22.7 ± 7.90	21.9	21.8 ± 7.31	27.3	26.7 ± 8.45	21.2	22.0 ± 7.94
Non-polar OMMs										
***n*-Alkanes**										
$\lg p^{o,*}_L$[c] > –8	2.72	3.26 ± 2.35	3.05	3.21 ± 1.76	0.54	1.96 ± 3.06	1.14	3.12 ± 5.02	0.56	1.24 ± 1.33
–10 < $\lg p^{o,*}_L$ < –8	6.76	11.1 ± 9.37	18.0	19.9 ± 8.99	9.56	13.2 ± 12.6	14.8	25.3 ± 27.2	9.75	12.7 ± 10.8
$\lg p^{o,*}_L$ < -10	28.1	32.1 ± 16.0	29.5	32.7 ± 18.2	19.8	25.5 ± 18.3	42.0	66.1 ± 53.8	20.7	24.5 ± 14.5
Subtotal	38.1	46.5 ± 25.9	52.6	55.8 ± 25.9	30.3	40.7 ± 32.2	63.3	96.0 ± 81.4	32.3	38.5 ± 24.7
PAHs										
$\lg p^{o,*}_L$ > –8	0.30	0.46 ± 0.52	0.31	0.48 ± 0.54	0.24	0.41 ± 0.52	0.41	0.70 ± 0.76	0.37	0.50 ± 0.53
-10 < $\log p^{o,*}_L$ < –8	1.04	1.49 ± 1.37	0.61	1.28 ± 1.41	0.95	1.50 ± 1.47	1.16	2.03 ± 2.03	1.29	1.79 ± 1.58
$\lg p^{o,*}_L$ < –10	4.20	5.03 ± 3.51	3.60	4.66 ± 3.93	4.82	5.94 ± 4.12	6.14	8.56 ± 7.55	6.02	6.77 ± 4.48
Subtotal	5.38	6.98 ± 5.19	4.43	6.42 ± 5.50	5.85	7.85 ± 5.77	7.85	11.3 ± 9.76	8.22	9.06 ± 6.33
oxy-PAHs										
$\lg p^{o,*}_L$ > –8	0.17	0.31 ± 0.38	0.13	0.27 ± 0.35	0.19	0.33 ± 0.38	0.24	0.40 ± 0.41	0.20	0.30 ± 0.30
$\lg p^{o,*}_L$ < –8	0.32	0.45 ± 0.43	0.38	0.47 ± 0.28	0.47	0.64 ± 0.50	0.58	0.86 ± 0.72	0.46	0.54 ± 0.44
Subtotal	0.51	0.76 ± 0.71	0.50	0.75 ± 0.58	0.66	0.97 ± 0.80	0.82	1.26 ± 1.03	0.67	0.84 ± 0.68
Steranes and hopanes	0.38	0.55 ± 0.48	0.78	0.98 ± 0.63	0.96	1.17 ± 0.92	1.99	3.31 ± 3.24	0.64	0.79 ± 0.53
Polar OMMs										
Isoprene SOA tracers	2.54	8.57 ± 18.3	2.25	5.68 ± 12.2	2.00	6.51 ± 14.6	2.38	6.29 ± 11.4	2.47	5.43 ± 9.11
a-Pinene SOA tracers	7.21	11.5 ± 10.7	7.18	9.94 ± 8.52	8.62	13.8 ± 13.7	6.04	10.3 ± 11.6	6.74	8.40 ± 7.00
Biomass burning tracers	82.5	128 ± 215	65.1	91.0 ± 73.2	87.4	115 ± 98.1	111	171 ± 159	99.3	132 ± 104
Sugar alcohols	7.56	9.01 ± 4.83	7.12	8.69 ± 5.63	6.34	8.19 ± 4.86	13.3	15.8 ± 9.32	9.89	10.7 ± 6.75
Saccharides	13.5	15.3 ± 7.43	13.3	15.4 ± 9.53	11.6	13.8 ± 7.83	19.0	23.6 ± 13.3	12.8	13.5 ± 5.90

[a] $rPM_{2.5} = NH_4^+ + K^+ + Ca^{2+} + NO_3^- + SO_4^{2-} + OC + EC$.
[b] $OC\% = OC/rPM_{2.5} \times 100\%$.
[c] Vapor pressure (atm) at 298.15 K based on values from Gou et al. (2021).

season is not primarily caused by local direct emissions, arguing for the establishment of joint prevention and control mechanisms at the regional level.

Fig. S1 shows that the concentrations of individual criteria air pollutants in the five cities also have similar temporal variations, and their COD values (0.09 ± 0.02–0.16 ± 0.03; Fig. 2b) suggest a high degree of similarity between the sampling sites. However, the *r* values of SO_2 concentrations (0.68 ± 0.11) were lower than those of other air pollutants (*r* = 0.81 ± 0.05–0.95 ± 0.03) and SO_4^{2-} (0.86 ± 0.05, Fig. 2a), supporting that SO_4^{2-} in $PM_{2.5}$ was not formed locally but during regional transport through atmospheric oxidation of SO_2 (van Donkelaar et al., 2008; He et al., 2012). Yu et al. (2020) and Xie et al. (2022b) found that the $PM_{2.5}$ mass in Nanjing city can be well reproduced by the sum of SNA, OC, and EC. Here, the $PM_{2.5}$ data collected for the five cities were in good agreement with $rPM_{2.5}$ (Fig. S4). These results validated our bulk speciation data and showed that $rPM_{2.5}$ can be used as a proxy measurement for $PM_{2.5}$ in the center of the Yangtze River Delta.

3.2. OMM composition

The median and mean concentrations of the measured OMM groups in the five cities are listed in Table 1. Tables S3 and S4 provide the median and mean concentrations of individual non-polar and polar OMMs, respectively. In all five cities, most *n*-alkanes and PAHs had a subcooled liquid vapor pressure at 298.15 K ($p^{o,*}_L$) of less than 10^{-10} atm, and these low-volatility compounds dominated the concentrations of total *n*-alkanes and total PAHs in $PM_{2.5}$ (Table 1); the total concentrations of oxygenated PAHs (oxy-PAHs) with $p^{o,*}_L < 10^{-8}$ atm (1,8-NAA, ATQ, and 7H-BANT) were also higher than those with $p^{o,*}_L > 10^{-8}$ atm (ACE, FLO, PHL-O, and XA; Table 1S and S3). Because the gas + particle phase concentrations of individual *n*-alkanes and PAHs generally follow a decreasing trend the lower the $p^{o,*}_L$ value in northern Nanjing (Gou et al., 2021), the dominance of low-volatility species for non-polar OMM groups in $PM_{2.5}$ is largely due to the evaporation of low molecular weight (MW) compounds. Although $PM_{2.5}$ sampling was conducted at urban sites in autumn and winter, high MW *n*-alkanes showed a clear predominance of odd over even chain lengths (C27 – C35; Table S3), indicating contributions from epicuticular wax in dust (Rogge et al., 1993b). Among the five cities, Changzhou had the highest concentrations of all non-polar OMM groups, particularly for high MW *n*-alkanes ($p^{o,*}_L < 10^{-10}$ atm), steranes, and hopanes, and was more affected by fossil fuel combustion and road dust.

As shown in Fig. 3, the biomass burning tracers had the highest percentage (mean ± stdev, 1.07 ± 0.38%–1.41 ± 0.66%) of organic matter (OM = 1.6 × OC), followed by high MW *n*-alkanes with $p^{o,*}_L < 10^{-10}$ atm (0.28 ± 0.098%–0.52 ± 0.31%) and saccharides (0.19 ± 0.12%–0.23 ± 0.13%). The secondary products of isoprene and α-pinene exhibited noticeable contributions (up to ~2%) to OM only in the first half of September, when biogenic VOC emissions and solar radiation were still intense. Sugar alcohols and saccharides are typical source markers for biological PM (Simoneit et al., 2004) and can also originate from biomass burning in winter (Marynowski and Simoneit, 2022; Feng et al., 2023; Cui et al., 2024). Similar to the non-polar OMMs, the highest average concentrations of biomass burning tracers, sugar alcohols, and saccharides were also observed at the Changzhou site (Table 1), where anthropogenic emissions exerted the greatest influence. The secondary products of isoprene and α-pinene reached their highest concentrations in Nanjing (8.57 ± 18.3 ng m^{-3}) and Wuxi (13.8 ± 13.7 ng m^{-3}), respectively, but not in Changzhou. In addition to the fact that the precursors of the measured SOA products were mainly from biogenic sources (Claeys et al., 2004, 2007; Szmigielski et al., 2007), this could also be partly due to the spatial homogeneity of SO_4^{2-} and NO_2 (Fig. 2),

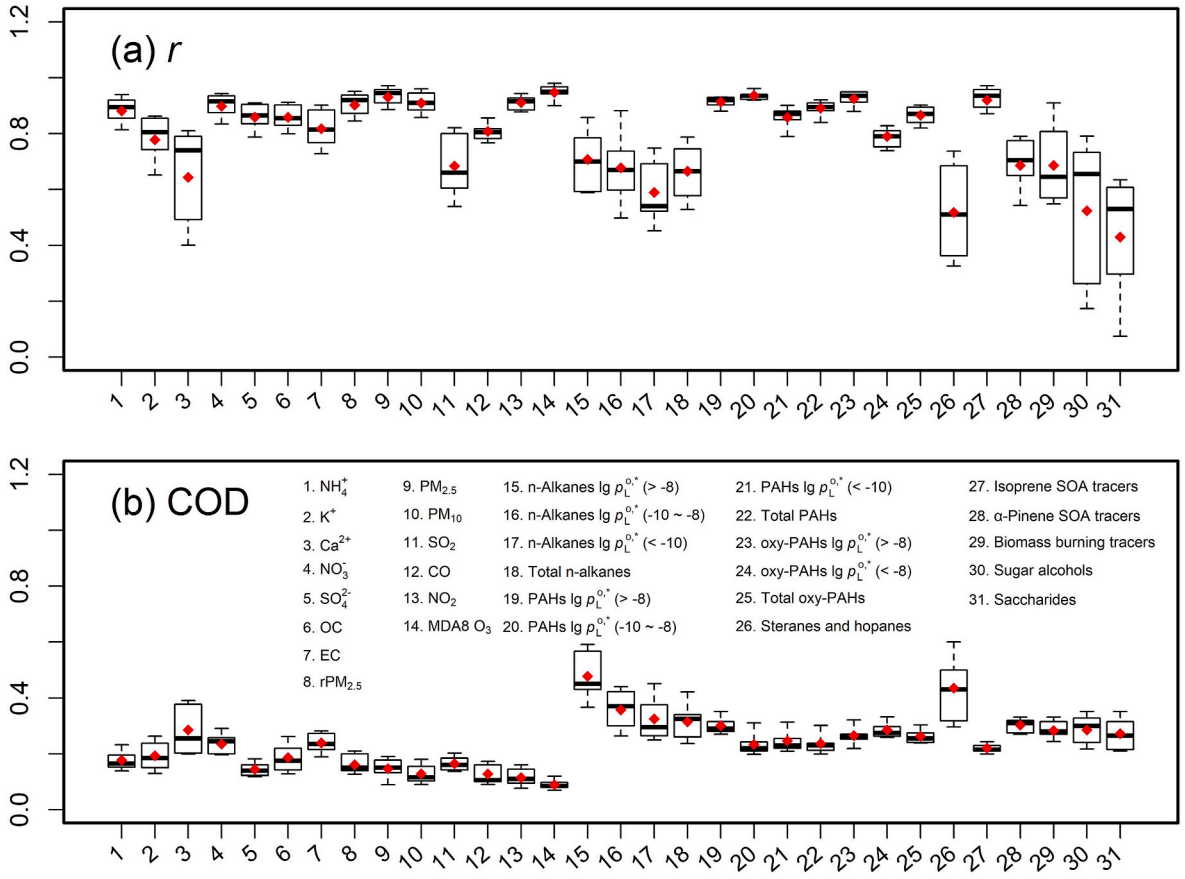

Fig. 2. Distribution of (a) correlation coefficients (*r*) and (b) coefficient of divergence (COD) for bulk $PM_{2.5}$ components, criteria air pollutants, and individual groups of OMMs between two sampling sites. The boxes depict the median (dark line), the inner quartile (box), the 10th and 90th percentiles (whiskers), and the mean (red diamond) of *r* and COD for 10 pairs of sampling sites. (For interpretation of the references to colour in this figure legend, the reader is referred to the Web version of this article.)

as the biogenic SOA derived from isoprene and monoterpenes can be mediated by anthropogenic sulfate and NO_X (Xu et al., 2015).

3.3. Spatiotemporal variations of OMMs

The temporal variations of the individual OMM groups in the five cities are illustrated in Figs. S5–S8. Fig. 2 visualizes the distribution of correlation coefficients (*r*) and COD for each OMM group between two sampling sites using boxplots. In general, the non-polar OMMs and biomass burning tracers reached their maximum concentrations in December 2020 and January 2021, which is due to the increasing use of biomass and fossil fuels and the low boundary layer height in winter. Concentrations of isoprene and α-pinene products showed a decreasing trend since September 2020 (Figs. S8a and b), as biogenic emissions and photochemical processes weakened after the end of summer. Compared to the temporal pattern of α-pinene SOA tracers, which continuously decreased from autumn to winter, isoprene products rapidly diminished to a minimum level from September to October 2020. Since isoprene and α-pinene are mainly emitted from deciduous and coniferous trees during the growing season, the temporal pattern of isoprene products may indicate a rapid decline in isoprene emissions due to the transition from the growing season to the dormant season of deciduous trees. Except for Changzhou, the sugar alcohols and saccharides in the other four cities did not show a clear temporal pattern (Figs. S8d and e). This is because sugar polyols are mainly derived from soil microorganisms and vegetation during the growing season and are affected by biomass burning in winter (Yttri et al., 2007; Verma et al., 2018).

Although the average concentrations of *n*-alkanes with $p^{o,*}_L > 10^{-8}$ atm were comparable in Nanjing (3.26 ± 2.35 ng m^{-3}), Suzhou (3.21 ± 1.76 ng m^{-3}), and Changzhou (3.12 ± 5.02 ng m^{-3}; Table 1), the Changzhou site showed much higher peak values on 12/21/2020 (31.3 ng m^{-3}) and November 01, 2021 (15.6 ng m^{-3}; Fig. S5a), when concentration peaks of *n*-alkanes with lower volatility ($p^{o,*}_L < 10^{-8}$ atm) also appeared (Figs. S5b and c). Due to the large intermittent peaks of *n*-alkanes with $p^{o,*}_L < 10^{-8}$ atm from November 2020 to January 2021 in Changzhou, their average concentrations were significantly higher ($p < 0.01$) than those in the other four cities. Considering that *n*-alkanes have multiple sources involving both biogenic emissions (e.g., plants and microorganisms; Rogge et al., 1993b, c) and anthropogenic activities (e.g., fossil fuel combustion, biomass burning, and cooking; Ren et al., 2020; Rogge et al., 1993a; Schauer et al., 1999, 2001, 2002), the wide ranges of *r* and COD values in Fig. 2 suggest considerable spatial heterogeneity of *n*-alkanes in all $p^{o,*}_L$ ranges during autumn and winter.

Unlike *n*-alkanes, the concentrations of PAHs and oxy-PAHs in the five cities exhibited a consistent temporal pattern, peaking in December 2020 and January 2021 (Figs. S6–S7). Moreover, PAHs and oxy-PAHs had high *r* (0.79 ± 0.050–0.94 ± 0.016; Fig. 2a) and low COD values (0.23 ± 0.048–0.30 ± 0.033; Fig. 2b) with narrow distributions. Given the strong correlation ($r > 0.90$, $p < 0.01$) between total PAHs and total oxy-PAHs in each city, both groups of OMMs were expected to originate mainly from incomplete combustion of fossil fuels and to be homogeneously distributed in the center of the Yangtze River Delta in autumn and winter. However, large between-site differences were observed at peak concentrations of PAHs and oxy-PAHs in winter, and Changzhou had significantly ($p < 0.01$) higher average concentrations of PAHs and oxy-PAHs than the other four cities (Table 1). One possible explanation

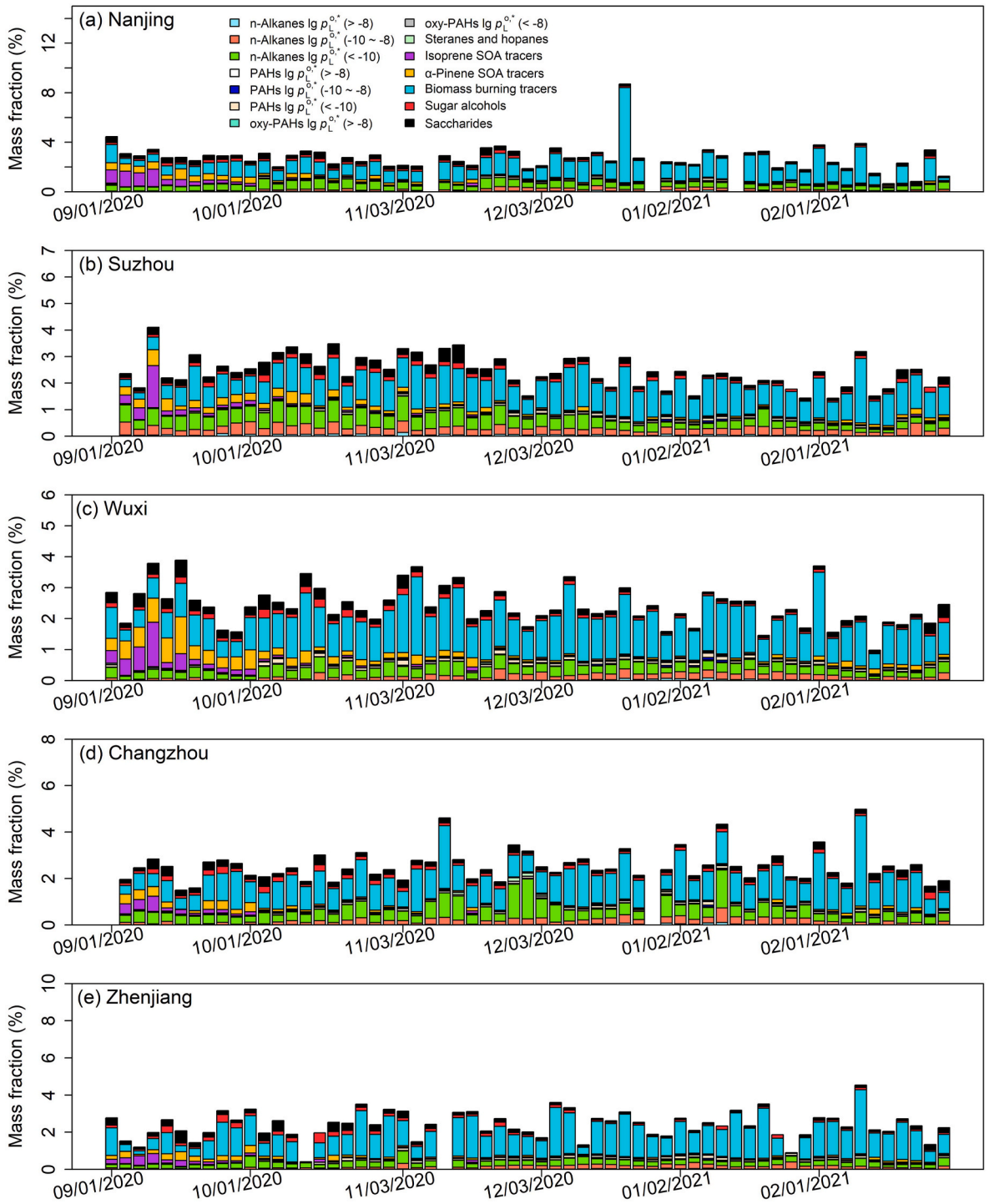

Fig. 3. Stacked time series of the contribution of each OMM group to organic matter (1.6 × OC) in (a) Nanjing, (b) Suzhou, (c) Wuxi, (d) Changzhou, and (e) Zhenjiang.

is that the sampling site in Changzhou is located near the industrial area in the northern part of the city, where large amounts of air pollutants were emitted and $PM_{2.5}$ pollution was severe in winter (Tao et al., 2021a, b). The intermittent PAH emissions from potential local sources (e.g., biomass burning, fireworks, and waste incineration) could also contribute to the differences between sites in the peak concentrations of PAHs in winter (Peng et al., 2016; Dat and Chang, 2017; Pongpiachan et al., 2017a, b). Steranes and hopanes are enriched in fuels and lubricants derived from crude oil and coal (Kaplan et al., 2001). Their concentrations were strongly correlated with low volatile *n*-alkanes ($p^{o,*}_L <$ 10^{-10} atm; $r > 0.65$) in the five cities, especially in Wuxi ($r = 0.88$) and Changzhou ($r = 0.80$). In Fig. 2, steranes and hopanes show a wide range of r values and the highest COD (0.44 ± 0.14). These results suggest a heterogeneous spatial distribution of hopanes and steranes in autumn and winter, which can be attributed to the difference in local emissions from motor vehicles and road dust.

Of all the OMM groups, the isoprene SOA tracers had the lowest average COD (0.22 ± 0.024) and a similar distribution of r values as PAHs and oxy-PAHs (Fig. 2). The homogeneous spatial distribution of isoprene products was probably due to their minimal formation after

September. While the α-pinene SOA tracers exhibited greater spatial variability with average *r* and COD values close to those of the total *n*-alkanes. This could be ascribed to the fact that α-pinene can also be emitted during biomass burning (Akagi et al., 2013). In this work, the biomass burning tracers showed moderate *r* values (0.53–0.91) and a narrow range of COD (0.19–0.34), indicating influences of both regional transport and local emissions. In the five cities, strong correlations ($r > 0.70$) between sugar polyols and biomass burning tracers were observed only in Suzhou and Changzhou. Due to the spatial variability of the contributing sources (biomass burning and biogenic emissions) of sugar alcohols and saccharides, their *r* values in Fig. 2a show the widest distributions.

3.4. PMF analysis

After testing PMF solutions with 4–10 factors, an 8-factor solution was finally chosen as having the most physically meaningful factors (Fig. S9). The error estimation results confirmed the robustness of the 4- to 9-factor solutions (Text S1 in Supporting Information and Table S2), and the Q/Q_{exp} value changed less with the factor number varying from 8 to 10 factors (9.01%–9.05%). In Table S5, the measurement data of $PM_{2.5}$ bulk species, particularly for the major components (SNA, OC, and EC), agree well with the PMF estimates. Thus, using an 8-factor solution to interpret the input data is appropriate. Referring to the dominant species in each factor profile (Fig. S9) and previous OMM-based source apportionment studies in Nanjing (Xie et al., 2022c; Feng et al., 2023), the resolved eight factors could be linked with biomass burning,

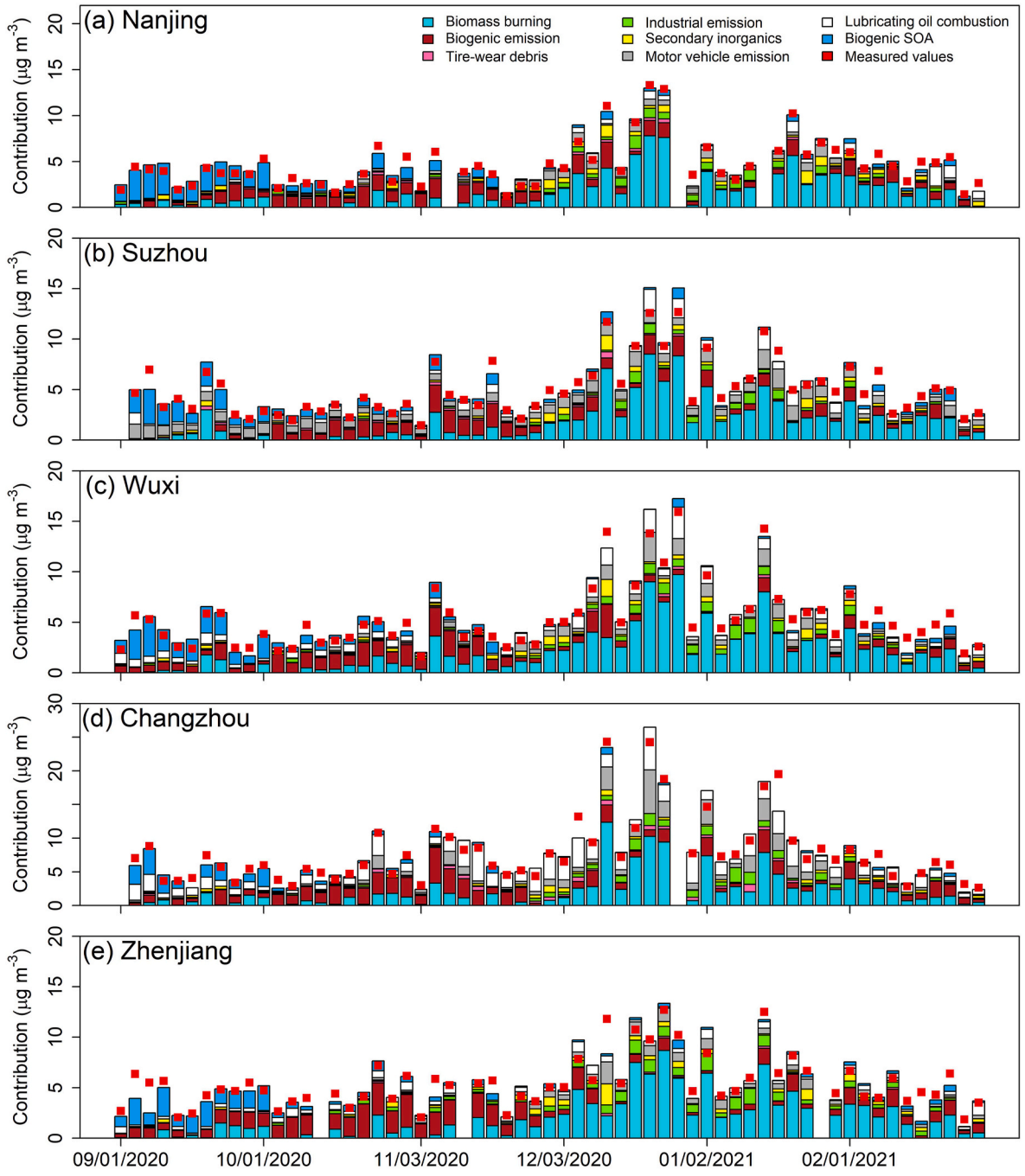

Fig. 4. Temporal variations of factor contribution distributions of OC in (a) Nanjing, (b) Suzhou, (c) Wuxi, (d) Changzhou, and (e) Zhenjiang.

biogenic emission, tire-wear debris, industrial emission, secondary inorganics, motor vehicle emission, lubricating oil combustion, and biogenic SOA. Their average contributions (%) to $PM_{2.5}$ major components in each city are shown in Table S6 in Supporting Information. The time series of the distribution of factors for the contribution of OC and total bulk components are shown in Fig. 4 and S10.

The biomass burning factor contained the largest proportion of galactosan, mannosan, and levoglucosan (53.9%–60.0%; Fig. S9a), which are typical byproducts of cellulose pyrolysis (Simoneit et al., 1999; Fabbri et al., 2009), and dominated the contributions to OC in December 2020 and January 2021 (Fig. 4). Its average relative contributions to OC and EC in the five cities were in the ranges of 27.9%–39.8% and 45.4%–57.9%, respectively (Table S6). Unlike the distribution of *r* values for the biomass burning tracers (Fig. 2a), the contributions of the biomass burning factor in the five cities showed strong correlations (r = 0.74–0.93, $p < 0.01$; Fig. 5a), indicating regional influences rather than local emissions. In addition to OC and EC, the contributions of the biomass burning factor at each site were also significantly correlated with NO_3^- (r = 0.63–0.81, $p < 0.01$) and $rPM_{2.5}$ (r = 0.66–0.87, $p <$ 0.01). Considering the high EC loading, the biomass burning factor was significantly affected by the long-range transport of biomass burning smoke and fossil fuel aerosols from residential heating in northern China in winter, and the use of clean energy (e.g., electricity and natural gas) should be increased to reduce emissions from winter heating. However, the influence of the aging process cannot be ruled out due to the lack of suitable organic tracers and source cycles (Hodshire et al., 2019; Qi and Wang, 2019).

The industrial emission, secondary inorganics, and biogenic SOA factors consisted mainly of PAHs, SNA, and secondary products of isoprene and α-pinene, respectively (Figs. S9d, e, and h). The contributions of all these three factors showed strong correlations (r = 0.85 ± 0.043–0.89 ± 0.070, $p < 0.01$) between the sampling sites (Fig. 5a), and only the biogenic SOA factor contributed significantly to OC and total bulk species in September (Fig. 4). In southern China, the increase of PAHs in winter was expected to be mainly caused by regional and local emissions from fossil fuel combustion (Yan et al., 2019). In this case, the strong correlations among sampling sites suggested the predominance of regional transport over local emissions, and the differences in local combustion sources and dispersion conditions across the five cities were responsible for the greater spatial heterogeneity of the industrial emission factor (COD = 0.46 ± 0.045) compared with the secondary inorganics (COD = 0.31 ± 0.053) and biogenic SOA factors (COD = 0.34 ± 0.047; Fig. 5b). Some of the input SOA products (e.g., 2-methyltetrols) may exist in the form of organosulfate by the reactive uptake of their gas-phase intermediates (e.g., isoprene epoxy diols; Surratt et al., 2010; Cui et al., 2018). In Fig. S9h, a notable fraction of SO_4^{2-} (24.1%) is probably incorrectly assigned to the biogenic SOA factor, which could be due to the fact that the PMF model assumes constant factor profiles and the diurnal cycles of the input species are not available. Unlike the biomass burning factor, the regional sources represented by these three factors were not the main contributors of the carbonaceous components in the five cities during autumn and winter (Table S6).

The biogenic emission factor was featured by significant proportions of sugar polyols (33.1%–55.1%) and also contained ~20% of biomass burning tracers (Fig. S9b). It dominated the contributions to OC from mid-September to mid-November in all five cities (Fig. 4). Besides the activities of microbiota and the decomposition of plant material in the soil, biomass burning also produces sugar polyols (Marynowski and Simoneit, 2022). In Fig. 5, the biogenic emission factor shows a broader *r* distribution (0.36–0.73) than the biomass burning factor with an average COD of 0.40 ± 0.024. Thus, this factor reflects combined contributions from local sources of soil resuspension and biomass burning in autumn and winter, which may explain the spatial heterogeneity of biomass burning tracers and sugar polyols (Fig. 2). Because the biomass burning and biogenic emission factors contained up to 28.8% of PAH compounds, regional transport and local emissions of biomass burning smoke were partly responsible for the elevated PAH levels in winter (Mandalakis et al., 2005; Pongpiachan, 2015, 2017a; Mao et al., 2018).

The tire-wear debris, motor vehicle emission, and lubricating oil combustion factors were characterized by high MW *n*-alkanes (*n*-C27–*n*-C35), *n*-alkanes with carbon numbers of 22–26, and steranes/hopanes, and were identified as traffic-related sources based on previous studies (Xie et al., 2013, 2022c; Feng et al., 2023). Among the five cities in southern Jiangsu, Suzhou had the highest number of motor vehicles (5.01 million) and highway passenger traffic (130 million) in 2022, followed by Nanjing and Wuxi (Jiangsu Provincial Bureau of Statistics of China, 2023), which cannot explain the highest contributions of traffic-related factors to OC (37.3%) and total bulk components (21.1%) at the Changzhou sampling site (Table S6). Several studies have found that the contributions of traffic-related factors and the concentrations of their source markers (e.g., steranes and hopanes) at each site are highly dependent on the surrounding traffic conditions (Xie et al., 2012a, b; Liu et al., 2013; Chow et al., 2022), and the three traffic-related factors identified in this study had lower mean *r* (0.27 ± 0.19–0.51 ± 0.16) and higher COD (0.47 ± 0.057–0.55 ± 0.10) values than other factors (Fig. 5). Even when their contributions in Changzhou were excluded for the spatial distribution analysis, these three traffic-related factors still exhibited greater spatial heterogeneity. Thus, the heterogeneous spatial distribution of traffic-related factors was caused by local emissions close to the sampling sites. As shown in Fig. 4, the motor vehicle emission and lubricating oil combustion factors have recognizable contributions to the total OC at its peak values in December and January, which can be mitigated by developing intelligent traffic management systems and promoting the adoption of new energy vehicles within each city (Guo et al., 2020b; Wang et al., 2021). Simply dividing the eight factors into two groups based on the distribution and mean values of their *r* values, regional sources, including biomass burning, industrial emission, secondary inorganics, and biogenic SOA, dominate the contributions to SNA (>80%) in all five cities. Except for Changzhou, where local emissions contributed more OC (55.7%) than regional transport, more

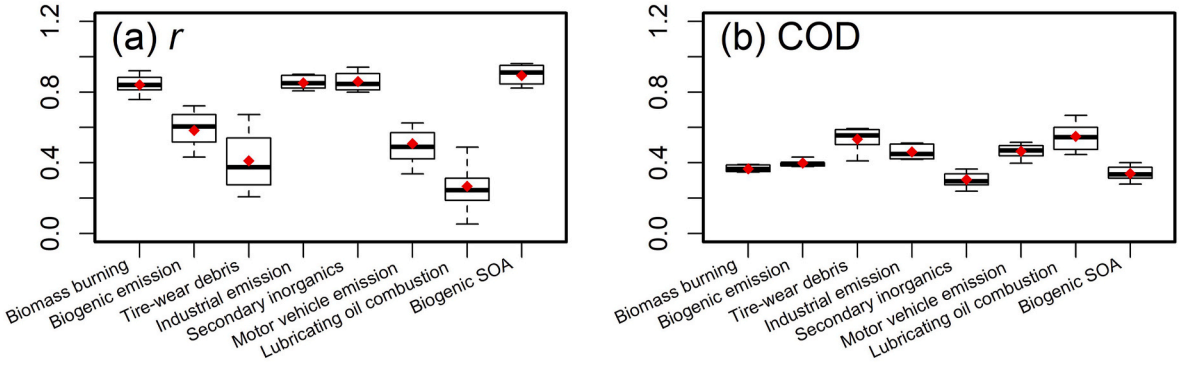

Fig. 5. Distribution of (a) *r* and (b) COD values for individual PMF factors between sampling sites.

than half of the OC in the other four cities came from regional sources (56.6%–65.6%) in autumn and winter.

4. Conclusions

According to the speciation results of $PM_{2.5}$ from Nanjing, Suzhou, Wuxi, Changzhou, and Zhenjiang, OC has the second highest relative contribution (18.7 ± 7.39%–26.7 ± 8.45%) to the total concentrations of measured bulk species during autumn and winter, indicating a necessity in controlling OA emission and formation to further reduce $PM_{2.5}$ pollution in the Yangtze River Delta. Low volatile *n*-alkanes and PAHs ($p^{o,*}_L < 10^{-10}$ atm) dominated the composition of identified non-polar OMMs in all five cities due to the evaporation of homologues with higher volatility; biomass burning tracers accounted for the highest percentages of OM for most of the sampling period; biogenic SOA products contributed significantly to OM during the first few sampling days at the end of summer. Similar to SNA and OC, PAHs and oxy-PAHs in different $p^{o,*}_L$ ranges and isoprene SOA tracers showed a homogeneous spatial distribution in autumn and winter, while other groups of OMMs exhibited greater spatial heterogeneity due to the influence of local emissions. A regional biomass burning factor, reflecting the transport of biomass burning smoke and fossil fuel aerosols in the heating season, was resolved by PMF analysis of $PM_{2.5}$ speciation data, and the contributions of traffic-related factors showed the largest spatial variability. The overall contributions of regional sources dominated OC concentrations in winter, supporting the implementation of joint prevention and control measures (e.g., clean energy use) to reduce OA emissions from residential heating. Effective regulatory strategies are also needed to control local traffic-related OA sources in the Yangtze River Delta.

CRediT authorship contribution statement

Wei Feng: Writing – original draft, Investigation, Data curation. **Guihong Dong:** Investigation, Data curation. **Wanqing Qi:** Visualization, Investigation. **Yizhen Wang:** Validation, Investigation. **Xiangyu Zhang:** Investigation. **Ke Li:** Writing – review & editing, Resources, Funding acquisition. **Hong Liao:** Writing – review & editing, Resources. **Yuhang Wang:** Writing – review & editing, Resources. **Zhijuan Shao:** Writing – review & editing. **Mingjie Xie:** Writing – review & editing, Supervision, Project administration, Methodology, Conceptualization.

Declaration of competing interest

The authors declare that they have no known competing financial interests or personal relationships that could have appeared to influence the work reported in this paper.

Acknowledgements

This work was supported by the National Key Research and Development Program of China (No. 2022YFE0136100) and the National Natural Science Foundation of China (NSFC, 42177211). We also thank the Nanjing Environmental Monitoring Center of Jiangsu Province for help with sampling.

Appendix A. Supplementary data

Supplementary data to this article can be found online at https://doi.org/10.1016/j.envpol.2024.125227.

Data availability

I have shared the link to my data in the manuscript

References

Akagi, S.K., Yokelson, R.J., Burling, I.R., Meinardi, S., Simpson, I., Blake, D.R., McMeeking, G.R., Sullivan, A., Lee, T., Kreidenweis, S., Urbanski, S., Reardon, J., Griffith, D.W.T., Johnson, T.J., Weise, D.R., 2013. Measurements of reactive trace gases and variable O3 formation rates in some South Carolina biomass burning plumes. Atmos. Chem. Phys. 13, 1141–1165. https://doi.org/10.5194/acp-13-1141-2013.

Cheung, K., Olson, M.R., Shelton, B., Schauer, J.J., Sioutas, C., 2012. Seasonal and spatial variations of individual organic compounds of coarse particulate matter in the Los Angeles Basin. Atmos. Environ. 59, 1–10. https://doi.org/10.1016/j.atmosenv.2012.05.037.

Chow, W.S., Huang, X.H.H., Leung, K.F., Huang, L., Wu, X., Yu, J.Z., 2022. Molecular and elemental marker-based source apportionment of fine particulate matter at six sites in Hong Kong, China. Sci. Total Environ. 813, 152652. https://doi.org/10.1016/j.scitotenv.2021.152652.

Claeys, M., Graham, B., Vas, G., Wang, W., Vermeylen, R., Pashynska, V., Cafmeyer, J., Guyon, P., Andreae, M.O., Artaxo, P., Maenhaut, W., 2004. Formation of secondary organic aerosols through photooxidation of isoprene. Science 303, 1173–1176. https://doi.org/10.1126/science.1092805.

Claeys, M., Szmigielski, R., Kourtchev, I., Van der Veken, P., Vermeylen, R., Maenhaut, W., Jaoui, M., Kleindienst, T.E., Lewandowski, M., Offenberg, J.H., Edney, E.O., 2007. Hydroxydicarboxylic acids: markers for secondary organic aerosol from the photooxidation of α-pinene. Environ. Sci. Technol. 41, 1628–1634. https://doi.org/10.1021/es0620181.

Cui, T., Zeng, Z., dos Santos, E.O., Zhang, Z., Chen, Y., Zhang, Y., Rose, C.A., Budisulistiorini, S.H., Collins, L.B., Bodnar, W.M., de Souza, R.A.F., Martin, S.T., Machado, C.M.D., Turpin, B.J., Gold, A., Ault, A.P., Surratt, J.D., 2018. Development of a hydrophilic interaction liquid chromatography (HILIC) method for the chemical characterization of water-soluble isoprene epoxydiol (IEPOX)-derived secondary organic aerosol. Environ. Sci. Process Impacts 20, 1524–1536. https://doi.org/10.1039/C8EM00308D.

Cui, W., Wang, Z., Feng, W., Qin, C., Liao, H., Wang, Y., Xie, M., 2024. Evaluating coarse PM composition and sources based on bulk and molecular speciation of PM2.5 and PM10 in Nanjing, East China. J. Environ. Sci. 152, 155–166. https://doi.org/10.1016/j.jes.2024.04.038.

Dat, N.-D., Chang, M.B., 2017. Review on characteristics of PAHs in atmosphere, anthropogenic sources and control technologies. Sci. Total Environ. 609, 682–693. https://doi.org/10.1016/j.scitotenv.2017.07.204.

Fabbri, D., Torri, C., Simoneit, B.R.T., Marynowski, L., Rushdi, A.I., Fabiańska, M.J., 2009. Levoglucosan and other cellulose and lignin markers in emissions from burning of Miocene lignites. Atmos. Environ. 43, 2286–2295. https://doi.org/10.1016/j.atmosenv.2009.01.030.

Feng, W., Wang, X., Shao, Z., Liao, H., Wang, Y., Xie, M., 2023. Time-resolved measurements of PM2.5 chemical composition and brown carbon absorption in Nanjing, East China: diurnal variations and organic tracer-based PMF analysis. J. Geophys. Res. Atmos. 128, e2023JD039092. https://doi.org/10.1029/2023JD039092.

Fourtziou, L., Liakakou, E., Stavroulas, I., Theodosi, C., Zarmpas, P., Psiloglou, B., Sciare, J., Maggos, T., Bairachtari, K., Bougiatioti, A., Gerasopoulos, E., Sarda-Estève, R., Bonnaire, N., Mihalopoulos, N., 2017. Multi-tracer approach to characterize domestic wood burning in Athens (Greece) during wintertime. Atmos. Environ. 148, 89–101. https://doi.org/10.1016/j.atmosenv.2016.10.011.

Golly, B., Waked, A., Weber, S., Samake, A., Jacob, V., Conil, S., Rangognio, J., Chrétien, E., Vagnot, M.P., Robic, P.Y., Besombes, J.L., Jaffrezo, J.L., 2019. Organic markers and OC source apportionment for seasonal variations of PM2.5 at 5 rural sites in France. Atmos. Environ. 198, 142–157. https://doi.org/10.1016/j.atmosenv.2018.10.027.

Gou, Y., Qin, C., Liao, H., Xie, M., 2021. Measurements, gas/particle partitioning, and sources of nonpolar organic molecular markers at a suburban site in the west Yangtze River Delta, China. J. Geophys. Res. Atmos. 126, e2020JD034080. https://doi.org/10.1029/2020JD034080.

Guo, B., Wang, Y., Zhang, X., Che, H., Zhong, J., Chu, Y., Cheng, L., 2020a. Temporal and spatial variations of haze and fog and the characteristics of PM2.5 during heavy pollution episodes in China from 2013 to 2018. Atmos. Pollut. Res. 11, 1847–1856. https://doi.org/10.1016/j.apr.2020.07.019.

Guo, Y., Tang, Z., Guo, J., 2020b. Could a smart city ameliorate urban traffic congestion? A quasi-natural experiment based on a smart city pilot program in China. Sustainability 12, 2291. https://doi.org/10.3390/su12062291.

Hallquist, M., Wenger, J.C., Baltensperger, U., Rudich, Y., Simpson, D., Claeys, M., Dommen, J., Donahue, N.M., George, C., Goldstein, A.H., Hamilton, J.F., Herrmann, H., Hoffmann, T., Iinuma, Y., Jang, M., Jenkin, M.E., Jimenez, J.L., Kiendler-Scharr, A., Maenhaut, W., McFiggans, G., Mentel, T.F., Monod, A., Prevot, A.S.H., Seinfeld, J.H., Surratt, J.D., Szmigielski, R., Wildt, J., 2009. The formation, properties and impact of secondary organic aerosol: current and emerging issues. Atmos. Chem. Phys. 9, 5155–5236.

He, H., Li, C., Loughner, C.P., Li, Z., Krotkov, N.A., Yang, K., Wang, L., Zheng, Y., Bao, X., Zhao, G., Dickerson, R.R., 2012. SO2 over central China: measurements, numerical simulations and the tropospheric sulfur budget. J. Geophys. Res. Atmos. 117, D00K37. https://doi.org/10.1029/2011JD016473.

Hodshire, A.L., Akherati, A., Alvarado, M.J., Brown-Steiner, B., Jathar, S.H., Jimenez, J.L., Kreidenweis, S.M., Lonsdale, C.R., Onasch, T.B., Ortega, A.M., Pierce, J.R., 2019. Aging effects on biomass burning aerosol mass and composition: a critical review of field and laboratory studies. Environ. Sci. Technol. 53, 10007–10022. https://doi.org/10.1021/acs.est.9b02588.

Huang, K., Zhuang, G., Li, J., Wang, Q., Sun, Y., Lin, Y., Fu, J.S., 2010. Mixing of Asian dust with pollution aerosol and the transformation of aerosol components during the dust storm over China in spring 2007. J. Geophys. Res. Atmos. 115, D00K13. https://doi.org/10.1029/2009JD013145.

Jaeckels, J.M., Bae, M.S., Schauer, J.J., 2007. Positive matrix factorization (PMF) analysis of molecular marker measurements to quantify the sources of organic aerosols. Environ. Sci. Technol. 41, 5763–5769. https://doi.org/10.1021/es062536b.

Jiangsu Provincial Bureau of Statistics of China, 2023. Jiangsu Statistical Yearbook 2023. China Statistics Press, Beijing (in Chinese). http://tj.jiangsu.gov.cn/2023/nj02/nj0210.htm.

Jimenez, J.L., Canagaratna, M.R., Donahue, N.M., Prevot, A.S.H., Zhang, Q., Kroll, J.H., DeCarlo, P.F., Allan, J.D., Coe, H., Ng, N.L., Aiken, A.C., Docherty, K.S., Ulbrich, I. M., Grieshop, A.P., Robinson, A.L., Duplissy, J., Smith, J.D., Wilson, K.R., Lanz, V.A., Hueglin, C., Sun, Y.L., Tian, J., Laaksonen, A., Raatikainen, T., Rautiainen, J., Vaattovaara, P., Ehn, M., Kulmala, M., Tomlinson, J.M., Collins, D.R., Cubison, M.J. E., Dunlea, J., Huffman, J.A., Onasch, T.B., Alfarra, M.R., Williams, P.I., Bower, K., Kondo, Y., Schneider, J., Drewnick, F., Borrmann, S., Weimer, S., Demerjian, K., Salcedo, D., Cottrell, L., Griffin, R., Takami, A., Miyoshi, T., Hatakeyama, S., Shimono, A., Sun, J.Y., Zhang, Y.M., Dzepina, K., Kimmel, J.R., Sueper, D., Jayne, J. T., Herndon, S.C., Trimborn, A.M., Williams, L.R., Wood, E.C., Middlebrook, A.M., Kolb, C.E., Baltensperger, U., Worsnop, D.R., 2009. Evolution of organic aerosols in the atmosphere. Science 326, 1525–1529. https://doi.org/10.1126/science.1180353.

Jo, D.S., Nault, B.A., Tilmes, S., Gettelman, A., McCluskey, C.S., Hodzic, A., Henze, D.K., Nawaz, M.O., Fung, K.M., Jimenez, J.L., 2023. Global health and climate effects of organic aerosols from different sources. Environ. Sci. Technol. 57, 13793–13807. https://doi.org/10.1021/acs.est.3c02823.

Kaplan, I.R., Lu, S.-T., Alimi, H.M., MacMurphey, J., 2001. Fingerprinting of high boiling hydrocarbon fuels, asphalts and lubricants. Environ. Forensics 2, 231–248. https://doi.org/10.1006/enfo.2001.0053.

Kim, E., Hopke, P.K., Pinto, J.P., Wilson, W.E., 2005. Spatial variability of fine particle mass, components, and source contributions during the regional air pollution study in St. Louis. Environ. Sci. Technol. 39, 4172–4179. https://doi.org/10.1021/es049824x.

Krudysz, M., Dutton, S., Brinkman, G., Hannigan, M., Fine, P., Sioutas, C., Froines, J., 2009. Intra-community spatial variation of size-fractionated organic compounds in Long Beach, California. Air Qual. Atmos. Hlth. 2, 69–88. https://doi.org/10.1007/s11869-009-0035-1.

Lewandowski, M., Jaoui, M., Offenberg, J.H., Kleindienst, T.E., Edney, E.O., Sheesley, R. J., Schauer, J.J., 2008. Primary and secondary contributions to ambient PM in the midwestern United States. Environ. Sci. Technol. 42, 3303–3309. https://doi.org/10.1021/es0720412.

Liu, J., Bergin, M., Guo, H., King, L., Kotra, N., Edgerton, E., Weber, R.J., 2013. Size-resolved measurements of brown carbon in water and methanol extracts and estimates of their contribution to ambient fine-particle light absorption. Atmos. Chem. Phys. 13, 12389–12404. https://doi.org/10.5194/acp-13-12389-2013.

Mandalakis, M., Gustafsson, Ö., Alsberg, T., Egebäck, A.-L., Reddy, C.M., Xu, L., Klanova, J., Holoubek, I., Stephanou, E.G., 2005. Contribution of biomass burning to atmospheric polycyclic aromatic hydrocarbons at three European background sites. Environ. Sci. Technol. 39, 2976–2982. https://doi.org/10.1021/es048184v.

Mao, S., Li, J., Cheng, Z., Zhong, G., Li, K., Liu, X., Zhang, G., 2018. Contribution of biomass burning to ambient particulate polycyclic aromatic hydrocarbons at a regional background site in East China. Environ. Sci. Technol. Lett. 5, 56–61. https://doi.org/10.1021/acs.estlett.8b00001.

Google Maps. Southern Jiangsu. https://earth.google.com/web/. (Accessed 25 May 2024).

Maria, S.F., Russell, L.M., Gilles, M.K., Myneni, S.C.B., 2004. Organic aerosol growth mechanisms and their climate-forcing implications. Science 306, 1921–1924. https://doi.org/10.1126/science.1103491.

Marynowski, L., Simoneit, B.R.T., 2022. Saccharides in atmospheric particulate and sedimentary organic matter: status overview and future perspectives. Chemosphere 288, 132376. https://doi.org/10.1016/j.chemosphere.2021.132376.

Mauderly, J.L., Chow, J.C., 2008. Health effects of organic aerosols. Inhal. Toxicol. 20, 257–288. https://doi.org/10.1080/08958370701866008.

Mukherjee, S., Dutta, M., Ghosh, A., Chatterjee, A., 2022. A year-long study on PM2.5 and its carbonaceous components over eastern Himalaya in India: contributions of local and transported fossil fuel and biomass burning during premonsoon. Environ. Res. 212, 113546. https://doi.org/10.1016/j.envres.2022.113546.

Nozière, B., Kalberer, M., Claeys, M., Allan, J., D'Anna, B., Decesari, S., Finessi, E., Glasius, M., Grgić, I., Hamilton, J.F., Hoffmann, T., Iinuma, Y., Jaoui, M., Kahnt, A., Kampf, C.J., Kourtchev, I., Maenhaut, W., Marsden, N., Saarikoski, S., Schnelle-Kreis, J., Surratt, J.D., Szidat, S., Szmigielski, R., Wisthaler, A., 2015. The molecular identification of organic compounds in the atmosphere: state of the art and challenges. Chem. Rev. 115, 3919–3983. https://doi.org/10.1021/cr5003485.

Padrón, J.D., Soler, D., Calafate, C.T., Cano, J.-C., Manzoni, P., 2022. Improving air quality in urban recreational areas through smart traffic management. Sustainability 14, 3445. https://doi.org/10.3390/su14063445.

Peng, N., Li, Y., Liu, Z., Liu, T., Gai, C., 2016. Emission, distribution and toxicity of polycyclic aromatic hydrocarbons (PAHs) during municipal solid waste (MSW) and coal co-combustion. Sci. Total Environ. 565, 1201–1207. https://doi.org/10.1016/j.scitotenv.2016.05.188.

Pongpiachan, S., 2015. Impacts of agricultural waste burning on the enhancement of PM 2.5-bound polycyclic aromatic hydrocarbons in northern Thailand, WIT Trans. Ecol. Environ. 198, 3–14. https://doi.org/10.2495/AIR150011.

Pongpiachan, S., Hattayanone, M., Cao, J., 2017a. Effect of agricultural waste burning season on PM2.5-bound polycyclic aromatic hydrocarbon (PAH) levels in Northern Thailand. Atmos. Pollut. Res. 8, 1069–1080. https://doi.org/10.1016/j.apr.2017.04.009.

Pongpiachan, S., Hattayanone, M., Suttinun, O., Khumsup, C., Kittikoon, I., Hirunyatrakul, P., Cao, J., 2017b. Assessing human exposure to PM10-bound polycyclic aromatic hydrocarbons during fireworks displays. Atmos. Pollut. Res. 8, 816–827. https://doi.org/10.1016/j.apr.2017.01.014.

Pye, H.O.T., Ward-Caviness, C.K., Murphy, B.N., Appel, K.W., Seltzer, K.M., 2021. Secondary organic aerosol association with cardiorespiratory disease mortality in the United States. Nat. Commun. 12, 7215. https://doi.org/10.1038/s41467-021-27484-1.

Qi, L., Wang, S., 2019. Fossil fuel combustion and biomass burning sources of global black carbon from GEOS-Chem simulation and carbon isotope measurements. Atmos. Chem. Phys. 19, 11545–11557. https://doi.org/10.5194/acp-19-11545-2019.

Qin, C., Gou, Y., Wang, Y., Mao, Y., Liao, H., Wang, Q., Xie, M., 2021. Gas–particle partitioning of polyol tracers at a suburban site in Nanjing, east China: increased partitioning to the particle phase. Atmos. Chem. Phys. 21, 12141–12153. https://doi.org/10.5194/acp-21-12141-2021.

Ren, L., Wang, Y., Kawamura, K., Bikkina, S., Haghipour, N., Wacker, L., Pavuluri, C.M., Zhang, Z., Yue, S., Sun, Y., Wang, Z., Zhang, Y., Feng, X., Liu, C.-Q., Eglinton, T.I., Fu, P., 2020. Source forensics of n-alkanes and n-fatty acids in urban aerosols using compound specific radiocarbon/stable carbon isotopic composition. Environ. Res. Lett. 15, 074007. https://doi.org/10.1088/1748-9326/ab8333.

Rogge, W.F., Hildemann, L.M., Mazurek, M.A., Cass, G.R., Simoneit, B.R.T., 1993a. Sources of fine organic aerosol .2. Noncatalyst and catalyst-equipped automobiles and heavy-duty diesel trucks. Environ. Sci. Technol. 27, 636–651. https://doi.org/10.1021/es00041a007.

Rogge, W.F., Hildemann, L.M., Mazurek, M.A., Cass, G.R., Simoneit, B.R.T., 1993b. Sources of fine organic aerosol .3. Road dust, tire debris, and organometallic brake lining dust - roads as sources and sinks. Environ. Sci. Technol. 27, 1892–1904. https://doi.org/10.1021/es00046a019.

Rogge, W.F., Hildemann, L.M., Mazurek, M.A., Cass, G.R., Simoneit, B.R.T., 1993c. Sources of fine organic aerosol .4. Particlulate abrasion products from leaf surfaces of urban plants. Environ. Sci. Technol. 27, 2700–2711. https://doi.org/10.1021/es00049a008.

Schauer, J.J., Kleeman, M.J., Cass, G.R., Simoneit, B.R.T., 1999. Measurement of emissions from air pollution sources. 2. C-1 through C-30 organic compounds from medium duty diesel trucks. Environ. Sci. Technol. 33, 1578–1587. https://doi.org/10.1021/es980081n.

Schauer, J.J., Kleeman, M.J., Cass, G.R., Simoneit, B.R.T., 2001. Measurement of emissions from air pollution sources. 3. C-1-C-29 organic compounds from fireplace combustion of wood. Environ. Sci. Technol. 35, 1716–1728. https://doi.org/10.1021/es001331e.

Schauer, J.J., Kleeman, M.J., Cass, G.R., Simoneit, B.R.T., 2002. Measurement of emissions from air pollution sources. 4. C-1-C-27 organic compounds from cooking with seed oils. Environ. Sci. Technol. 36, 567–575. https://doi.org/10.1021/es002053m.

Shrivastava, M.K., Subramanian, R., Rogge, W.F., Robinson, A.L., 2007. Sources of organic aerosol: positive matrix factorization of molecular marker data and comparison of results from different source apportionment models. Atmos. Environ. 41, 9353–9369. https://doi.org/10.1016/j.atmosenv.2007.09.016.

Simoneit, B.R.T., Schauer, J.J., Nolte, C.G., Oros, D.R., Elias, V.O., Fraser, M.P., Rogge, W.F., Cass, G.R., 1999. Levoglucosan, a tracer for cellulose in biomass burning and atmospheric particles. Atmos. Environ. 33, 173–182. https://doi.org/10.1016/S1352-2310(98)00145-9.

Simoneit, B.R.T., Elias, V.O., Kobayashi, M., Kawamura, K., Rushdi, A.I., Medeiros, P.M., Rogge, W.F., Didyk, B.M., 2004. Sugars dominant water-soluble organic compounds in soils and characterization as tracers in atmospheric particulate matter. Environ. Sci. Technol. 38, 5939–5949. https://doi.org/10.1021/es0403099.

Sun, J., Gong, J., Zhou, J., Liu, J., Liang, J., 2019. Analysis of PM2.5 pollution episodes in Beijing from 2014 to 2017: classification, interannual variations and associations with meteorological features. Atmos. Environ. 213, 384–394. https://doi.org/10.1016/j.atmosenv.2019.06.015.

Surratt, J.D., Chan, A.W.H., Eddingsaas, N.C., Chan, M., Loza, C.L., Kwan, A.J., Hersey, S. P., Flagan, R.C., Wennberg, P.O., Seinfeld, J.H., 2010. Reactive intermediates revealed in secondary organic aerosol formation from isoprene. Proc. Natl. Acad. Sci. U.S.A. 107, 6640–6645. https://doi.org/10.1073/pnas.0911114107.

Szmigielski, R., Surratt, J.D., Gómez-González, Y., Van der Veken, P., Kourtchev, I., Vermeylen, R., Blockhuys, F., Jaoui, M., Kleindienst, T.E., Lewandowski, M., Offenberg, J.H., Edney, E.O., Seinfeld, J.H., Maenhaut, W., Claeys, M., 2007. 3-methyl-1,2,3-butanetricarboxylic acid: an atmospheric tracer for terpene secondary organic aerosol. Geophys. Res. Lett. 34, L24811. https://doi.org/10.1029/2007GL031338.

Tao, Y., Sun, N., Li, X., Zhao, Z., Ma, S., Huang, H., Ye, Z., Ge, X., 2021a. Chemical and optical characteristics and sources of PM2.5 humic-like substances at industrial and suburban sites in Changzhou, China. Atmosphere 12, 276. https://doi.org/10.3390/atmos12020276.

Tao, Y., Yuan, Y., Cui, Y., Zhu, L., Zhao, Z., Ma, S., Ye, Z., Ge, X., 2021b. Comparative analysis of the chemical characteristics and sources of fine atmospheric particulate matter (PM2.5) at two sites in Changzhou, China. Atmos. Pollut. Res. 12, 101124. https://doi.org/10.1016/j.apr.2021.101124.

Urban, R.C., Lima-Souza, M., Caetano-Silva, L., Queiroz, M.E.C., Nogueira, R.F.P., Allen, A.G., Cardoso, A.A., Held, G., Campos, M.L.A.M., 2012. Use of levoglucosan, potassium, and water-soluble organic carbon to characterize the origins of biomass-

burning aerosols. Atmos. Environ. 61, 562–569. https://doi.org/10.1016/j.atmosenv.2012.07.082.
van Donkelaar, A., Martin, R.V., Leaitch, W.R., Macdonald, A.M., Walker, T.W., Streets, D.G., Zhang, Q., Dunlea, E.J., Jimenez, J.L., Dibb, J.E., Huey, L.G., Weber, R., Andreae, M.O., 2008. Analysis of aircraft and satellite measurements from the Intercontinental Chemical Transport Experiment (INTEX-B) to quantify long-range transport of East Asian sulfur to Canada. Atmos. Chem. Phys. 8, 2999–3014. https://doi.org/10.5194/acp-8-2999-2008.
Verma, S.K., Kawamura, K., Chen, J., Fu, P., 2018. Thirteen years of observations on primary sugars and sugar alcohols over remote Chichijima Island in the western North Pacific. Atmos. Chem. Phys. 18, 81–101. https://doi.org/10.5194/acp-18-81-2018.
Wang, L., Chen, X., Zhang, Y., Li, M., Li, P., Jiang, L., Xia, Y., Li, Z., Li, J., Wang, L., Hou, T., Liu, W., Rosenfeld, D., Zhu, T., Zhang, Y., Chen, J., Wang, S., Huang, Y., Seinfeld, J.H., Yu, S., 2021. Switching to electric vehicles can lead to significant reductions of PM2.5 and NO2 across China. One Earth 4.
Wang, J., 2013. China Air Quality Online Monitoring and Analysis Platform. http://www.aqistudy.cn. (Accessed 10 April 2024).
Wei, W., Wang, S., Hao, J., Cheng, S., 2011. Projection of anthropogenic volatile organic compounds (VOCs) emissions in China for the period 2010–2020. Atmos. Environ. 45, 6863–6871. https://doi.org/10.1016/j.atmosenv.2011.01.013.
Wu, Z., Zhang, X., Wu, M., 2016. Mitigating construction dust pollution: state of the art and the way forward. J. Clean. Prod. 112, 1658–1666. https://doi.org/10.1016/j.jclepro.2015.01.015.
Xie, M., Coons, T.L., Dutton, S.J., Milford, J.B., Miller, S.L., Peel, J.L., Vedal, S., Hannigan, M.P., 2012a. Intra-urban spatial variability of PM2.5-bound carbonaceous components. Atmos. Environ. 60, 486–494. https://doi.org/10.1016/j.atmosenv.2012.05.041.
Xie, M., Coons, T.L., Hemann, J.G., Dutton, S.J., Milford, J.B., Peel, J.L., Miller, S.L., Kim, S.-Y., Vedal, S., Sheppard, L., Hannigan, M.P., 2012b. Intra-urban spatial variability and uncertainty assessment of PM2.5 sources based on carbonaceous species. Atmos. Environ. 60, 305–315. https://doi.org/10.1016/j.atmosenv.2012.06.036.
Xie, M., Piedrahita, R., Dutton, S.J., Milford, J.B., Hemann, J.G., Peel, J.L., Miller, S.L., Kim, S.-Y., Vedal, S., Sheppard, L., Hannigan, M.P., 2013. Positive matrix factorization of a 32-month series of daily PM2.5 speciation data with incorporation of temperature stratification. Atmos. Environ. 65, 11–20. https://doi.org/10.1016/j.atmosenv.2012.09.034.
Xie, M., Feng, W., He, S., Wang, Q.g., 2022a. Seasonal variations, temperature dependence, and sources of size-resolved PM components in Nanjing, east China. J. Environ. Sci. 121, 175–186. https://doi.org/10.1016/j.jes.2021.12.022.
Xie, M., Lu, X., Ding, F., Cui, W., Zhang, Y., Feng, W., 2022b. Evaluating the influence of constant source profile presumption on PMF analysis of PM2.5 by comparing long- and short-term hourly observation-based modeling. Environ. Pollut. 314, 120273. https://doi.org/10.1016/j.envpol.2022.120273.
Xie, M., Peng, X., Shang, Y., Yang, L., Zhang, Y., Wang, Y., Liao, H., 2022c. Collocated measurements of light-absorbing organic carbon in PM2.5: observation uncertainty and organic tracer-based source apportionment. J. Geophys. Res. Atmos. 127, e2021JD035874. https://doi.org/10.1029/2021JD035874.
Xu, L., Guo, H., Boyd, C.M., Klein, M., Bougiatioti, A., Cerully, K.M., Hite, J.R., Isaacman-VanWertz, G., Kreisberg, N.M., Knote, C., Olson, K., Koss, A., Goldstein, A.H., Hering, S.V., de Gouw, J., Baumann, K., Lee, S.-H., Nenes, A., Weber, R.J., Ng, N.L., 2015. Effects of anthropogenic emissions on aerosol formation from isoprene and monoterpenes in the southeastern United States. Proc. Natl. Acad. Sci. U.S.A. 112, 37–42. https://doi.org/10.1073/pnas.1417609112.
Yan, D., Wu, S., Zhou, S., Tong, G., Li, F., Wang, Y., Li, B., 2019. Characteristics, sources and health risk assessment of airborne particulate PAHs in Chinese cities: a review. Environ. Pollut. 248, 804–814. https://doi.org/10.1016/j.envpol.2019.02.068.
Yang, Y., Christakos, G., Yang, X., He, J., 2018. Spatiotemporal characterization and mapping of PM2.5 concentrations in southern Jiangsu Province, China. Environ. Pollut. 234, 794–803. https://doi.org/10.1016/j.envpol.2017.11.077.
Yang, L., Shang, Y., Hannigan, M.P., Zhu, R., Wang, Q.g., Qin, C., Xie, M., 2021. Collocated speciation of PM2.5 using tandem quartz filters in northern Nanjing, China: sampling artifacts and measurement uncertainty. Atmos. Environ. 246, 118066. https://doi.org/10.1016/j.atmosenv.2020.118066.
Yttri, K.E., Dye, C., Kiss, G., 2007. Ambient aerosol concentrations of sugars and sugar-alcohols at four different sites in Norway. Atmos. Chem. Phys. 7, 4267–4279. https://doi.org/10.5194/acp-7-4267-2007.
Yu, Y., Ding, F., Mu, Y., Xie, M., Wang, Q.g., 2020. High time-resolved PM2.5 composition and sources at an urban site in Yangtze River Delta, China after the implementation of the APPCAP. Chemosphere 261, 127746. https://doi.org/10.1016/j.chemosphere.2020.127746.
Zhang, Y.-L., Cao, F., 2015. Fine particulate matter (PM2.5) in China at a city level. Sci. Rep. 5, 14884. https://doi.org/10.1038/srep14884.
Zhang, Q., Jimenez, J.L., Canagaratna, M.R., Allan, J.D., Coe, H., Ulbrich, I., Alfarra, M. R., Takami, A., Middlebrook, A.M., Sun, Y.L., Dzepina, K., Dunlea, E., Docherty, K., DeCarlo, P.F., Salcedo, D., Onasch, T., Jayne, J.T., Miyoshi, T., Shimono, A., Hatakeyama, S., Takegawa, N., Kondo, Y., Schneider, J., Drewnick, F., Borrmann, S., Weimer, S., Demerjian, K., Williams, P., Bower, K., Bahreini, R., Cottrell, L., Griffin, R.J., Rautiainen, J., Sun, J.Y., Zhang, Y.M., Worsnop, D.R., 2007. Ubiquity and dominance of oxygenated species in organic aerosols in anthropogenically-influenced Northern Hemisphere midlatitudes. Geophys. Res. Lett. 34, L13801. https://doi.org/10.1029/2007GL029979.
Zhang, T., Liu, P., Sun, X., Zhang, C., Wang, M., Xu, J., Pu, S., Huang, L., 2020. Application of an advanced spatiotemporal model for PM2.5 prediction in Jiangsu Province, China. Chemosphere 246, 125563. https://doi.org/10.1016/j.chemosphere.2019.125563.
Zhang, C., Xu, T., Wu, G., Gao, F., Liu, Y., Gong, D., Wang, H., Zhang, C., Wang, B., 2022. Reduction of fugitive VOC emissions using leak detection and repair (LDAR) in a petroleum refinery of Pearl River Delta, China. Appl. Energy 324, 119701. https://doi.org/10.1016/j.apenergy.2022.119701.
Zheng, M., Ke, L., Edgerton, E.S., Schauer, J.J., Dong, M., Russell, A.G., 2006. Spatial distribution of carbonaceous aerosol in the southeastern United States using molecular markers and carbon isotope data. J. Geophys. Res. Atmos. 111, D10S06. https://doi.org/10.1029/2005JD006777.
Zheng, H., Wan, X., Kang, S., Chen, P., Li, Q., Maharjan, L., Guo, J., 2024. Molecular characterization of organic aerosols over the Tibetan Plateau: spatiotemporal variations, sources, and potential implications. Environ. Pollut. 340, 122832. https://doi.org/10.1016/j.envpol.2023.122832.
Zhou, D., Ding, K., Huang, X., Liu, L., Liu, Q., Xu, Z., Jiang, F., Fu, C., Ding, A., 2018. Transport, mixing and feedback of dust, biomass burning and anthropogenic pollutants in eastern Asia: a case study. Atmos. Chem. Phys. 18, 16345–16361. https://doi.org/10.5194/acp-18-16345-2018.